16th World Conference on Earthquake Engineering, 16WCEE 2017
Santiago Chile, January 9th to 13th 2017
Paper N° 2994
Registration Code: S-O1464708203

PROBABILISTIC SEISMIC HAZARD ANALYSIS FOR CHILE

F. Medina,(1) S.C. Harmsen,(2) and S.E. Barrientos(3)

(1) *Principal, FME Engineering, San Francisco, California, USA, francisco@cal.berkeley.edu.*
(2) *Scientist, US Geological Survey, Golden, Colorado, USA.*
(3) *Director, Centro Sismológico Nacional, Universidad de Chile, Santiago, Chile.*

Abstract

A probabilistic seismic hazard analysis (PSHA) of Chile is presented, based on a newly assembled homogeneous and complete catalog of unique and independent (Poissonian) seismic events affecting Chile. All seismogenic zones present in Chile are included in the model: subduction, shallow, intermediate, deep, and outer-rise seismicity, and the main Quaternary faults located within the country or in close proximity to its borders (in Argentina, Bolivia, and Peru). The effect of the Chile triple junction at the Taitao Peninsula is considered, and consequently is reflected in the results obtained. The PSHA included: (a) Gutenberg-Richter rate of exceedance models developed for all the seismogenic zones considered; (b) the most up-to-date ground-motion prediction models available for the seismogenic zones considered; and (c) both, a rupture model and the three-dimensional geometry of the subduction slab. Several features of the model were verified with three recent events: (1) 2005 Tarapacá, Mw=7.9; (2) 2010 Maule, Mw=8.8; and (3) 2014 Iquique, Mw=8.2. The results show good agreement with the data observed. Disaggregation of the probabilities of exceedance show that most of the risk is due to magnitude 7.8 or greater subduction events, located at approximately 40 km from the considered sites. The hazard is finally expressed in terms of peak ground acceleration and spectral acceleration maps at 10% and 2% probability of exceedance in 50 years for Continental and Insular Chile, suitable for seismic code applications. These maps include Eastern and Salas y Gómez Islands, Desventuradas Archipelago (San Ambrosio and San Félix Islands), Juan Fernández Archipelago, the southern tip of Peru, southwestern Bolivia, and western Argentina.

Keywords: Probabilistic seismic hazard analysis; subduction hazard; Chile seismic hazard; Chilean seismic code; Western Argentina seismic hazard.

1. Introduction

Chile is one of the most affected countries by strong destructive subduction earthquakes, usually followed by equally destructive tsunamis. Chile is also affected by other strong seismic events with different seismogenesis (shallow, intermediate depth and deep earthquakes, outer-rise, crustal faults, and volcanic-activity-triggered earthquakes). Chile's historical and instrumental seismic record recently exhibited an unprecedented period; within a short time, three earthquakes of large magnitude occurred: the 2010 Maule (Mw=8.8), 2014 Iquique (Mw=8.1), and 2015 Illapel (Mw=8.4) events. The closest analogous spike in strong seismic activity, was the 1960 Valdivia earthquake (Mw=9.5) followed by two strong aftershocks the day after (Mw=7.9 and 8.1). This earthquake activity has generated, within the Chilean engineering community, review of the existing seismic codes for building structures [1], NCh433, and industrial structures [2]. Another code used in highway projects is the Chilean Public Works Ministry's *Highway Manual* [3]. An emergency addendum to NCh433 was rushed [4], and then replaced [5] within a year. Currently, an *ad-hoc* committee is looking at the codes with a longer and deeper view.

1.1 Background

A brief presentation, of a more detailed probabilistic seismic hazard analysis (PSHA) of Chile [6], is herein outlined. The seismicity affecting Chile's national continental and insular territories were studied for all seismogenic sources. This characterization was based on: (a) the most relevant information found, over a large quantity of bibliographical material available; (b) process and analysis of the historical and instrumental seismicity that occurred in Chile and 200 km beyond its borders, assembled in a catalog obtained from the

University of Chile's National Seismological Center, augmented with data from the US Geological Survey (USGS)'s National Earthquake Information Center, the United Kingdom's based International Seismological Centre, and the SISRA catalog [7]; (c) theoretical and empirical seismology and engineering related to Chile's seismicity; and (d) experience with Chile's historical and recorded seismicity. The resulting model was used to carry out a PSHA for the national territory. The results of the PSHA express the seismic demand, in terms of maximum peak and pseudo-spectral ground accelerations (PGA and pSA, respectively), due to the seismicity affecting all sites within Chile for a given probability of exceedance. This PSHA includes: (a) regional tectonics, geology and seismicity; (b) expected maximum magnitudes and corresponding return periods generated by known sources and faults; (c) attenuation characteristics of the seismic waves from the source to the sites; and (d) near-source effects. The Chilean codes mentioned do not prescribe the seismic demand in this fashion, as other codes do it; for example, the International Building Code [8], the American Society of Civil Engineers' ASCE7 code [9], and others. The PSHA results obtained are presented as an alternative to consider for prescribing the seismic demand over Chile's national territory. The PSHA was carried out using accepted state-of-the-art technologies, first proposed by Cornell [10] and subsequently applied to USA's national territory by the USGS [11]. The USGS has been improving, expanding, and updating these procedures every six years (1996, 2002, 2008, and 2014) [12], resulting in time-independent hazard maps implemented into USA seismic codes.

The hazard maps developed provide the latest integrated data for future ground motions, solidly based in science, with a long history of analysis, revision and discussion in the engineering and scientific communities.

1.2 Previous studies

A preliminary regional seismic hazard model for South America was developed [13], including a smoothed seismicity component applied across the entire continent that accounts for earthquakes in the magnitude (M) range 5 to 7, subduction zone sources (M=7.0-9.5), and crustal faults sources (M=7.0-8.0). Other features of the model include the epistemic consideration of ground motion models. The model, however, lacks sufficient resolution. Other more detailed seismic hazard analyses over part of Chile, north of the Taitao Peninsula, have been carried out [14-15]. These analyses are compared to the present study elsewhere [6].

1.3 Methodology validation

The results were verified using PGAs recorded in three recent earthquakes: 2005 Tarapacá (Mw=7.9), 2010 Maule (Mw=8.8), and 2014 Iquique (Mw=8.2) [6]. A good correlation was observed between the results obtained from the model and the accelerations recorded in the field. The implied slip rate for the model's mega-thrust earthquakes was also satisfactorily compared with plate convergence rates measured geodetically.

2. Seismological and Theoretical Background

2.1 Chile seismicity and seismological data

Continental Chile has been, and is, conditioned by a convergent margin of tectonic plates, the most important being the subduction of the Nazca plate under the South American plate between Arica, from the north, and the triple junction close to the Taitao Peninsula, to the south. This subduction process has generated, and is capable of generating, seismic events of great magnitude, which in turn cause tsunamis with great damage potential along Chile's coastline. Two recent events stand out: (1) the 1960 Valdivia earthquake, which generated the most important tsunami on Chile's coasts during the XX Century, in terms of damage and wave run-ups; and (2) the 2010 Maule earthquake, which generated one of the most destructive tsunamis that have occurred in Chile.

The catalog assembled was used to characterize the main seismogenic zones affecting Chile. These zones are defined by the seismic events occurring on the interface of the subduction plate (interplate events), away from the interface within the plates (intraplate events) at shallow, intermediate and deep depths, in the crust close to the surface, and on the outer-rise mainly affecting Insular Chile. The data were collected into a single catalog of close to 12,000 seismic events with homogeneous moment magnitude satisfying completeness, uniqueness, and independence. The catalog was partitioned into the defined seismogenic zones for which seismic productivity rate models were developed up to an expected maximum magnitude. A number of active Quaternary faults within Chile borders and a few in neighboring countries were also included in the model.

2.2 Probabilistic seismic hazard analysis (PSHA)

2.2.1 Introduction. Following Cornell [10], future earthquakes are characterized by size, frequency, location, and the ground motion that they are likely to produce. The method assumes that earthquake ruptures occur independently from one another, allowing the analysis to combine hazard from different sources into a single hazard curve. Thus, a probability of ground motion exceedance can be associated with each seismic source in the hazard model. (A series of independent Poisson random variables may be added, and the sum is also a Poisson random variable with mean equal to the sum of the individual component means, $\lambda=\sum\lambda_i$.) The ground motion considered in this work is the PGA or the pSA (*SA* hereafter). The *SA* logarithm is assumed normally distributed for a given magnitude, distance to the source, *R*, and other controlling source (and site) parameters.

2.2.2 Earthquake probability for the seismic hazard model. The seismic hazard model contains mean annual earthquake rate information for all the model's considered sources. Sources are described as finite ruptures (fault or subduction event) or point sources (background seismicity). Annual rate of occurrence information is collected at each site, if a given source is within *k* horizontal or map distance from site S. The mean annual rate of each source with magnitude M±0.05 and distance less than *k* from S is added to yield a scalar value at S. Earthquake probability maps for sources with k<50 km from each site were developed (sampled at 0.1° in latitude and longitude). All of these conditional earthquakes rates (for a given M and k<50 km from site S) are then added to obtain the mean annual frequency exceeding M. These rates are converted to probability of exceeding M in the time interval of interest *T* (years). If λ is the annual frequency of exceedance, the conditional probability is

$$\Pr[m > \mathrm{M}, r < R, t = T] = 1 - e^{-T\lambda} \quad (1)$$

For example, Fig. 1 shows probabilities of exceedance maps using a randomly chosen period of 30-year time spans. There is no record of large earthquakes (M>8.0) east of Chile's Central Valley. This is reflected in the center-right and far-right panels on Fig. 1. This figure includes the latest developments to treat subduction sources: two logic-tree branches are considered, one where the interface rupture surface stops at the Taitao Triple Junction (branch weight 0.8), and the other where the interface may continue rupturing as far south as 52.5° S (branch weight 0.2).

2.2.3 Seismic hazard model theoretical background. Let S_i be a single hazard source, independent from any other, with mean annual rate λ_i; then, the mean annual rate of exceeding a given *SA* is

$$\mathrm{R_{ex}}(\mathrm{SA}|\mathrm{S_i}) = \lambda(\mathrm{S_i}) \int_{\ddot{x}_0}^{\ddot{x}_{\max}} \Pr[\ddot{x}|\mathrm{M_i}, \mathrm{r_i}, \mathrm{site}, \ldots] d\ddot{x} \quad (2)$$

where M_i, r_i, and site respectively are the magnitude of S_i, the distance to the site, the site condition (average shear wave propagation velocity in the top 30 m of the soil column under the site; type of subsoil: soil, rock, sedimentary basin depth, etc.), and other physical factors that influence ground motion (such as sense of slip, depth of source, etc.). The dots, …, represent other factors, such as source mechanism, source depth, and source directivity, known to affect the strength of ground motion during an earthquake. The integrated variable, $\ddot{x}$, is the *SA* logarithm, and Pr is $\ddot{x}$'s probability density function. In empirical studies, Pr is best fit by the normal probability density function, with mean and standard deviation, σ, functions of the aforementioned controlling factors. The lower limit, $\ddot{x}_0$, is defined as the logged *SA* that produces a given mean rate of exceedance. The upper limit, $\ddot{x}_{\max}$, is defined as the mean +3σ; that is, the distribution is truncated at three standard deviations above the logged mean motion [12, 16].

The mean hazard is computed by a weighted sum over the epistemic alternatives. In this work several ground motion models are considered for each source type. Epistemic uncertainty is also considered on source features, such as mean annual rate, source mechanism, and so on. The epistemic alternatives should be in some sense a representation of the diversity of reasonably informed professional opinion about future earthquake and ground motion characteristics given the geology and tectonic setting of Chile. The PSHA model accommodates these assumptions as epistemic alternatives with weights that capture the relative confidence strength. In theory, epistemic uncertainty decreases over time, as continued investigation and scientific advance reduces the range of plausible future scenarios.

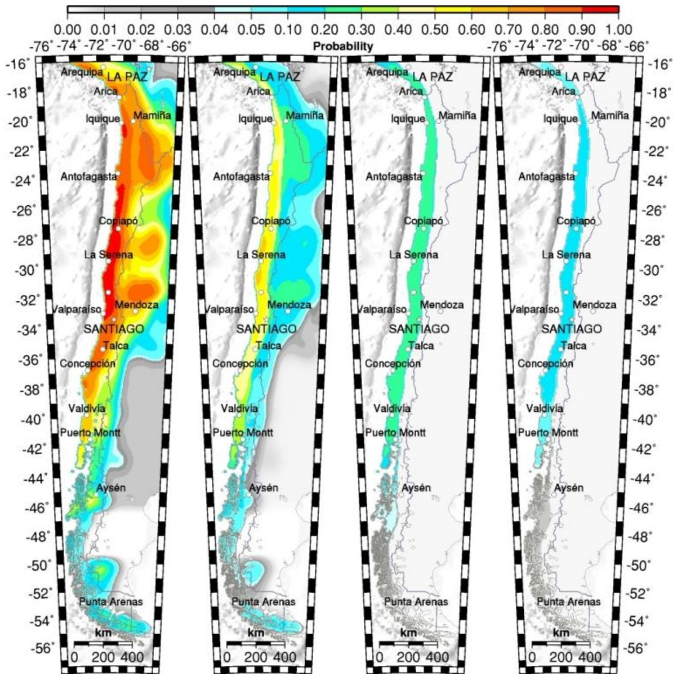

Figure 1 – Probability of moderate to large earthquakes within 50 km of each location in a random 30-year period. Panels left to right: earthquakes M≥6.0, M≥7.0, M≥8.0, and M≥9.0.

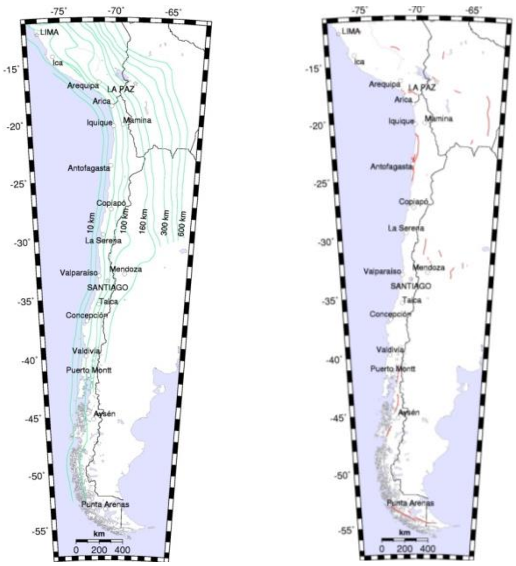

(a) (b)

Figure 2 – (a) Three-dimensional Chile subduction surface. Green contour lines represent depth to interface at 10, 20, 50, 80, 100, 160, 200, 300, 400, 500, and 600 km; 10- and 50-km contour lines are extended to 52.5° S for this study. (b) Active Quaternary faults (traces colored red) in Chile and neighboring areas of Argentina, Bolivia, and Peru.

The minimum magnitude of interest is taken as 5.0 and the greatest distance as 200 km for crustal sources and 500 to 1,000 km for subduction earthquakes. Although smaller and more distant sources may sometimes be felt, they are generally considered to potentially cause damage. Exceptions, such as very shallow sources with magnitudes less than 5.0, are sometimes found causing damage in the immediate epicenter locality, but these are generally omitted, with few exceptions, because larger sources generally cover for them.

For the entire ensemble of sources, S_i (i=1,2,…,n), the aggregate rate of exceedance is

$$R_{ex}(SA|S_i) = \sum_1^n R_{ex}(SA|S_i) \tag{3}$$

The rate of exceedance is a Poisson-distributed random variable; therefore, the probability of exceedance, PE, is

$$\mathrm{PE}(SA) = 1 - e^{-R_{ex}(SA)T} \tag{4}$$

For example, for the seismic demand on infrastructure commonly defined as the Maximum Design Earthquake, such that it is exceeded 10% of the time by seismic events occurring during a period of 50 years (a 475-year return-period event), the SA is found from

$$0.10 = 1 - e^{-R_{ex}(SA)50} \tag{5}$$

3. Model Characterization

3.1 Geometry of seismogenic zones

Descriptions and characterizations of the seismogenic zones considered and the effects of the associated seismic events are presented elsewhere [6, 17]. The main and best-studied source occurs due to the subduction of the Nazca plate below the South American plate. A three-dimensional surface geometry for South America subduction zone has been developed [18] by interpolating approximately 600 individual two-dimensional profiles, along the strike of the subduction zone, obtained from recorded seismic data, and a number of field-measured active-source seismic profiles (Fig. 2a). In southern Chile, the extent of this geometry is limited, due to a lack of significant subduction related seismicity. To extend the reach of the hazard model developed for this project, a 50-km-depth contour line has been defined for the slab surface parallel to the trench. In addition to the subduction seismogenic zone, the seismic hazard model includes: (a) interplate south of Chile triple junction; (b) shallow, intermediate, and deep intraplate; (c) outer-rise (west of the Peru-Chile Trench); and (d) crustal.

Most of Chile's crustal faults deform very slowly; thus, the influence on hazard from these faults is subtle. One exception is the Magallanes-Fagnano Fault System, with about 6 to 7 mm/yr and less than 1,000 year mean recurrence time for characteristic events. In general, the crustal faults mean annual rates for characteristic events are of the order of 10^{-4}, for mean recurrence intervals of about 10,000 years. Hazard maps corresponding to 500 to 2,500 year return periods would not be much influenced by such faults. Only Quaternary faults with published characterization parameters are explicitly modeled in this study [19-21]: Atacama (Punta de Lobos, Salar del Carmen North and South, Sierra de Remiendos), Morro Mejillones, Cerro Gordo, Cerro Moreno, Cerro Fortuna, San Ramón [22], Liquiñe-Ofqui (Reloncaví, Hornopirén, Puyuhuapi, San Rafael), Río San Juan, Magallanes-Fagnano (Western and Eastern Sections). The model also includes Quaternary faults from Argentina (Comechingones El Molino Branch, El Tigre, Las Chacras, Los Berros, Maradona-Acequión, San Luis), Bolivia (Río Beni, Este de Peñas, Mandeyapecua, Tarija, Tunari), and Peru (Chaspaya, Machado Chico, Quiches, Cuzco) [20, 23-24]. These faults are close to the boundary with Chile (Fig. 2b). Of these latter faults, only Argentina's El Tigre and Las Chacras have a significant slip rate, 3 mm/yr.

3.2 Frequency-magnitude (Gutenberg-Richter) relationships

Seismic productivity rates are characterized by the Gutenberg-Richter (GR) relationship [25],

$$\log(N) = A - b\mathrm{M} \tag{6}$$

where N (or N_{EQ}) is the number of earthquakes with magnitude larger or equal to M, A is the number of seismic events with magnitude larger than 0 per units of time and of area, and b is the ratio between the number of low- over large-magnitude events. Usually, the value of b is around one; systematic deviations from this number are interpreted as belonging to regions in extreme states of stress or to swarm-like activity.

3.2.1 Historical seismic catalog data to earthquake frequencies. The homogenized moment magnitude catalog data are run through a Gardner and Knopoff (GK) filter [26] to remove foreshocks and aftershocks. The GK algorithm's time-space windows, developed for M<8 earthquakes, were extrapolated using world-wide data to identify aftershocks from large subduction and deep earthquakes [27]. The time window for M=9.5 was set at 2,400 days (>6 years); the corresponding distance window was defined as the 1960 Valdivia earthquake rupture length. For the largest sources, the original algorithm circular spatial zones were replaced with elongated or rectangular zones (Table 1). These windows need to be revised as recent data suggest aftershocks may occur during longer periods. However, the GK algorithm used filters out most of the aftershocks. One notable earthquake, labeled an "aftershock" of the Maule mega-thrust, but correctly identified as a crustal event [28-29] is the M=7.0 Pichilemu normal-focus event of 11 March 2010, 14:55 UTC. The Maule main shock may have triggered this crustal event; however, the GK algorithm's spatial window for the Maule main shock did not extend into the Pichilemu epicentral region. The magnitude 6.9 Pichilemu event that occurred a few minutes earlier is discarded by the algorithm as a foreshock of the 14:55 main shock.

Table 1 – Time and distance windows used on Chile seismic catalog to eliminate dependent events.

M	5.0	5.5	6.0	6.5	7.0	7.5	8.0	8.5	9.0	9.5
***t* (days)**	155	290	510	790	915	960	985	1,200	1,600	2,400
***R* (km)**	40	47	54	61	70	81	94	100	200	-

The resulting catalog, called cleaned catalog, is processed to determine activity rates and b-values of nominally independent earthquake sources, using the maximum likelihood method for an assumed GR magnitude and frequency distribution. The cumulative seismicity rates are determined by counting earthquakes in each 0.1° by 0.1° grid cell, accounting for variable catalog completeness using Stepp's algorithm [30]. Sensitivity to the minimum magnitude used to determine the rates was checked against historical rates, and revised if needed. Finally, a smoothed catalog is obtained by redistributing the earthquakes from their point-source locations to two-dimensional symmetric Gaussian distributions with mean value at the event epicenter (shifted to nearest cell center) and 50 km of standard deviation.

3.2.2 Source-specific Gutenberg-Richter relationships. Upon partition of Chile's seismicity data, based on the zones' seismogenic characteristics and using the cleaned and complete catalog, linear semi-log regressions were carried out to obtain GR relationships for each seismogenic zone.

The interplate zone records activity on the interface between the Nazca and South America plates. The great 1960 Valdivia earthquake (M_w=9.5) is an example of the interplate seismicity that it is included in the PSHA model. The catalog begins with a M=8.5 event on 11 November 1922, the Vallenar subduction earthquake, which left over 1,000 people dead, including those killed by the generated tsunami. An earlier event, the 16 December 1575 Valdivia earthquake (M=9.0-9.5), is also considered among the largest mega-thrust events. It produced a tsunami wave that ran up the Valdivia River and caused landslides and flooded the town [31], much like the 1960 Valdivia earthquake. Fig. 3 shows the earthquake expected counts for this model on an annualized basis. A tapered GR relationship for M>9.5 is used. The taper is included to limit the frequency computed by extrapolating the GR relationship; thus, reducing the predicted rate of extremely large mega-thrust events, such that the slip falls within the bounds available from GPS plate convergence rates. The GR curve developed fits the bulk of the data well. The uncertainty in determining the annual event frequency is expressed as a factor of 2 around the predicted value (Fig. 3, red vertical bar), limiting the upper bound to a 410-year return period, or 0.00244 times/year. Fig. 4 shows the probability of one or more events M=5.0-7.8, per 0.1°×0.1° cell in a random 100-year period, associated with interplate seismicity. This figure shows concentrated hazard in specific places that have experienced higher rates of such earthquakes in the past. The seismic part of the deformation is modeled as a mix of reverse slip (75%) and strike slip (25%).

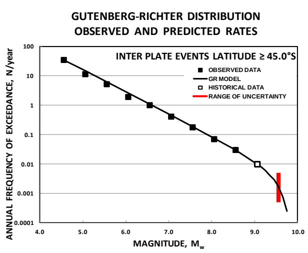

Figure 3 – Expected cumulative interplate activity rates. Data and model correspond to the primary branch extending to 45° S for M≥4.5.

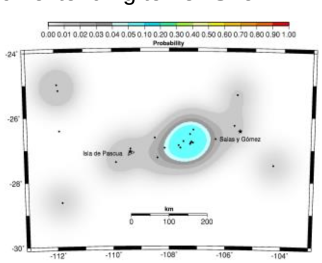

Figure 6 – Probability of a M≥5.0 event affecting Easter and Salas y Gómez Islands, in a random 100-year period per 0.1°×0.1° cell. Dots are epicenters from the catalog used.

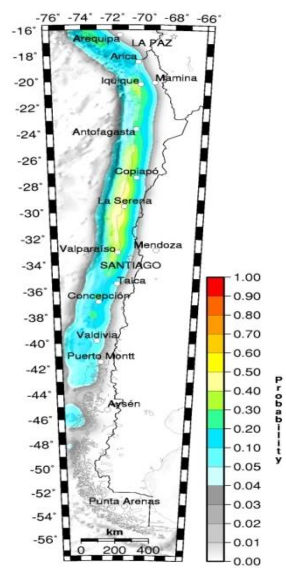

Figure 4 – Probability of a 5.0≤M≤7.8 interplate event, in a random 100-year period per 0.1°×0.1° cell. Model considers rupture to extend south, beyond the triple junction.

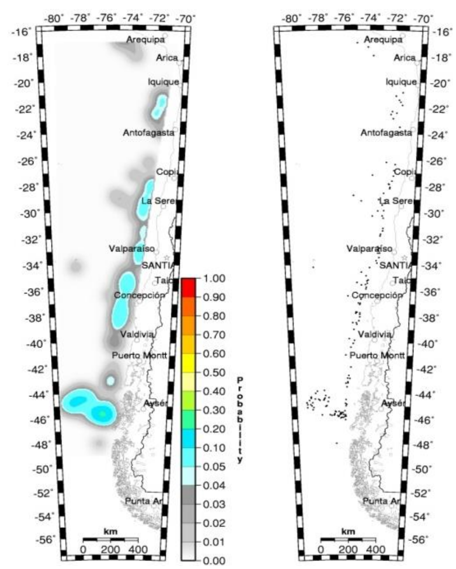

Figure 5 – Probability of a M≥5.0 outer-rise event, in a random 100-year period per 0.1°×0.1° cell (left panel). Outer-rise seismicity, according to the catalog between 1923 and 2012 (right panel).

Similar analyses were carried out for the other seismogenic zones considered: (a) shallow intraplate seismicity; (b) southern Chile; (c) onshore intermediate depth and deep seismicity; (d) offshore (outer-rise) seismicity (see Fig. 5); and (e) Easter and Salas y Gómez Islands (Fig. 6), and Juan Fernández Archipelago.

3.3 Maximum magnitudes

The seismogenic zones include an estimation of the maximum magnitude that earthquakes can reach within its limits. This is the Maximum Credible Earthquake (MCE), the largest earthquake that appears to be possible in a given tectonic environment (interplate, intraplate, crustal). The largest ever instrumentally-recorded earthquake in the world took place in Chile: the M=9.5, 1960 Valdivia earthquake. The rupture started at the hypocenter, at 30 to 40 km-depth beneath the Arauco Peninsula, and extended for nearly 1,000 km southward to the Taitao Peninsula. The maximum displacement along the fault reached 40 m [32], generating a sea-floor elevation change significant enough to produce a 15 m tsunami at Mocha Island. Other large earthquakes, according to the extent and description of damage, tsunami characteristics, main-shock duration in minutes, time extent of aftershocks in months/years, etc., have allowed investigators to identify the largest events in past centuries. Earthquakes taking place in 1575, 1730, 1868, 1877, 1922, and 2010 are probably the largest ones in recent history, apart from the 1960 event. The 1575 and 1730 are probably magnitude 9+ events, while 1868, 1877, and 2010 are close to magnitude 9.

In summary, the maximum magnitude to consider in the coupling region is 9.5 to 9.8 between the Arauco and Taitao Peninsulas, and 9.0 to 9.2 from the Arauco Peninsula to the north. MCEs in the intraplate seismogenic zone at intermediate depth should be 7.8 to 8.0 from 33° S to the south and north of 26° S. Between 26° and 33° S the MCE for the intermediate depth events should be around 7.5.

3.4 Interplate rupture modeling

Large interplate earthquakes occurring in Chile are modeled as scenario events that step along the interface at 6-km increments from the northernmost to the southernmost edge of the subducting zone considered (15.5° to 45° S). Two subduction zones are considered, as described above. The ridge between the Nazca and Antarctic plates is considered a barrier to through going rupture in the main subduction model, with weight 0.8. However, the model admits that subduction sources may rupture past the triple junction to 52.5° S, using the alternate subduction model with weight 0.2, because the Chile ridge has subducted [33]. The size of these interplate subduction events ranges in magnitude from 7.8 to 9.8. Earthquakes with magnitude less than 7.8 are abundant in this zone, but are not constrained to lie on the interface in the PSHA model. Fig. 7 shows three of the relationships considered to model rupture length [34-36].

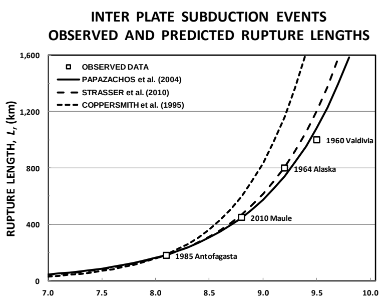

Figure 7 – Expected and observed interplate rupture lengths for subduction events.

The May 1960 Great Chilean Earthquake had a rupture length of approximately 900 to 1,000 km [32, 37], in better agreement with Papazachos relationship [36]. The 1964 Great Alaska Earthquake, M=9.2, had an approximate rupture length of 800 km [38], again in better agreement with said relationship. The M=8.1 Antofagasta earthquake of 1995 had a rupture length of about 180 km [39], in agreement with all the relationships. The M=8.8 Maule earthquake of 2010 had a rupture length of 450 km [40], in good agreement with Papazachos'. This relationship [36] was the one most supported by actual Chilean data; thus, this model was used with full weight (1.0).

The largest modeled event is only expected to rupture a fraction of the Nazca plate total subduction length, 3,503 km (4,375 km when including Antarctic plate subduction). For example, for the May 1960 Valdivia earthquake, the Papazachos relationship yields a 1,084 km mean rupture length, or 31% of the total available on the Nazca plate. Details on Chile's interplate scenarios when using this relationship are shown in Table 2.

3.5 Rupture slip and convergence rates

The Nazca plate is converging with the South American plate in a slightly north of east direction, with a mean relative rate of about 70 mm/year in the north and about 65 mm/year in the south [40]. The convergence rate is constrained by the total seismic moment rate budget,

$$\dot{M}_0 = \mu A_r \dot{s}; \quad A_r(\mathrm{M}) = L_r(\mathrm{M})W \tag{7}$$

where μ is the subduction slab rigidity, A_r and L_r, respectively are the area and length of the rupture zone, functions of magnitude, and W is the rupture width whose horizontal component, W_H, is given an average value of 150 km, assuming a rupture width of 1.55° longitude interval at 30° S. Then, the average horizontal slip rate per scenario is

$$\dot{s}_H = {\dot{M}_0}\Big/{(\mu L_r W_H)} \tag{8}$$

To convert earthquake rates, the primary input to the seismic-hazard model (Table 2), to slip rates, an average value of the slab rigidity (μ=500 kilobars) is assumed over the down-dip rupture. The depth range for these earthquakes is 10 to 50 km. This average value for circum-Pacific subduction zones (including Chile) is consistent with the PREM model [41].

Table 2 – Expected interplate rupture scenarios for subduction events, based on Papazachos relationship [36].

MAGNITUDE M_w	RUPTURE PER SCENARIO LENGTH L, km	RUPTURE PER SCENARIO LENGTH %	FREQUENCY N_{EQ}/yr	SCENARIOS TOTAL N_T	SCENARIOS RATIO*10^5 (N_{EQ}/N_T)/yr
7.85	134	3.80%	0.018310	562	3.2581
7.95	152	4.30%	0.015392	559	2.7535
8.05	173	4.90%	0.012939	556	2.3272
8.15	196	5.60%	0.010877	552	1.9704
8.25	223	6.40%	0.009143	548	1.6685
8.35	253	7.20%	0.007686	543	1.4155
8.45	287	8.20%	0.006461	537	1.2032
8.55	325	9.30%	0.005431	531	1.0228
8.65	369	10.50%	0.004566	523	0.8730
8.75	419	12.00%	0.003838	515	0.7452
8.85	476	13.60%	0.003226	506	0.6376
8.95	540	15.40%	0.002712	495	0.5479
9.05	613	17.50%	0.002280	483	0.4720
9.15	696	19.90%	0.001916	469	0.4086
9.25	790	22.50%	0.001611	453	0.3556
9.35	896	25.60%	0.001354	435	0.3113
9.45	1,017	29.00%	0.001138	415	0.2743
9.55	1,155	33.00%	0.000580	392	0.1481
9.65	1,311	37.40%	0.000296	366	0.0809
9.75	1,488	42.50%	0.000151	337	0.0448

Table 3 – Expected interplate rupture slip rates for subduction events in three locations in Chile, based on Papazachos relationship [36].

CITY	IQUIQUE				VALPARAÍSO				VALDIVIA			
MAGNITUDE, M_w	NUMBER OF SCENARIOS, N_{IQQ}	ANNUAL FREQUENCY RATE, (N_{IQQ}/N_T)/yr	SEISMIC MOMENT RATE $\dot{M}_0$*10^{-18}, Nm/yr	HORIZONTAL SLIP RATE $\dot{s}_H$, mm/yr	NUMBER OF SCENARIOS, N_{VAL}	ANNUAL FREQUENCY RATE, (N_{VAL}/N_T)/yr	SEISMIC MOMENT RATE $\dot{M}_0$*10^{-18}, Nm/yr	HORIZONTAL SLIP RATE $\dot{s}_H$, mm/yr	NUMBER OF SCENARIOS, N_{VIA}	ANNUAL FREQUENCY RATE, (N_{VIA}/N_T)/yr	SEISMIC MOMENT RATE $\dot{M}_0$*10^{-18}, Nm/yr	HORIZONTAL SLIP RATE $\dot{s}_H$, mm/yr
7.85	23	0.000749	0.50	0.51	23	0.000749	0.50	0.51	23	0.000749	0.50	0.51
7.95	26	0.000716	0.68	0.61	26	0.000716	0.68	0.61	26	0.000716	0.68	0.61
8.05	29	0.000675	0.90	0.71	30	0.000698	0.93	0.74	29	0.000675	0.90	0.71
8.15	33	0.000650	1.22	0.85	34	0.000670	1.26	0.88	33	0.000650	1.22	0.85
8.25	37	0.000617	1.64	1.01	38	0.000634	1.69	1.04	37	0.000617	1.64	1.01
8.35	42	0.000594	2.23	1.21	43	0.000609	2.29	1.24	43	0.000609	2.29	1.24
8.45	48	0.000578	3.07	1.46	49	0.000590	3.13	1.49	48	0.000578	3.07	1.46
8.55	55	0.000563	4.22	1.77	55	0.000563	4.22	1.77	55	0.000563	4.22	1.77
8.65	62	0.000541	5.73	2.12	62	0.000541	5.73	2.12	62	0.000541	5.73	2.12
8.75	70	0.000522	7.81	2.55	71	0.000529	7.92	2.58	70	0.000522	7.81	2.55
8.85	80	0.000510	10.78	3.10	80	0.000510	10.78	3.10	80	0.000510	10.78	3.10
8.95	90	0.000493	14.72	3.73	91	0.000499	14.88	3.77	90	0.000493	14.72	3.73
9.05	102	0.000481	20.30	4.53	103	0.000486	20.50	4.57	92	0.000434	18.31	4.09
9.15	116	0.000474	28.23	5.55	117	0.000478	28.48	5.60	92	0.000376	22.39	4.40
9.25	132	0.000469	39.50	6.84	132	0.000469	39.50	6.84	92	0.000327	27.53	4.77
9.35	137	0.000427	50.69	7.74	150	0.000467	55.50	8.47	92	0.000286	34.04	5.19
9.45	137	0.000376	63.09	8.48	170	0.000466	78.29	10.53	92	0.000252	42.37	5.70
9.55	137	0.000203	48.10	5.70	193	0.000286	67.77	8.03	92	0.000136	32.30	3.83
9.65	137	0.000111	37.11	3.87	219	0.000177	59.32	6.19	92	0.000074	24.92	2.60
9.75	137	0.000061	29.02	2.67	220	0.000099	46.61	4.29	92	0.000041	19.49	1.79
AGGREGATE SLIP RATE				65.01				74.36				52.03

The convergence rate is compared with an estimate of mean horizontal slip rate from large to great subduction earthquakes predicted by the seismic-hazard model in Table 3. This table shows the slip rates and number of scenarios, N_{EQ}, associated with magnitude 7.85 to 9.75 events that rupture directly under three cities in Chile: Iquique, Valparaíso, and Valdivia. It can be seen that in Iquique about 65 mm/yr of horizontal slip is accounted for by these large subduction earthquakes, while in Valparaíso and Valdivia about 74 and 52 mm/yr are respectively accounted for. In Valparaíso, about 25% of the calculated slip rate comes from magnitude 9.55 to 9.75 earthquakes that rupture under the city. Even though these are exceedingly rare events, their large seismic moments and the relatively large number of scenarios that rupture under the city make these mega-thrust sources very important components of the hazard model. In both, northern and southern Chile, about 70 to 80% of the convergence rate is accounted for by seismic slip on large to great subduction earthquakes in the model, given the assumptions discussed above (Table 4, final row). The remaining 30 to 20% is partly accounted for from smaller earthquakes whose contributions have not been tabulated, but is mostly unaccounted for (aseismic slip, after-slip, aftershocks). The PSHA concerns itself with independent events, and specifically omits foreshocks and aftershocks, which may in some instances contribute significantly to the total seismic-moment budget.

4. Acceleration Attenuation Relationships

Several hundred models have been developed to predict strong-motion PGA, based on empirical data from acceleration records processed statistically [42]. These models are generically called ground motion prediction equations or ground motion models (GMMs). However, there have not been developed, well validated models from Chilean data satisfying four essential conditions: (1) well characterized seismogenic sources; (2) well distributed strong-motion instrument-recording network able to capture occurring strong motions with fidelity; (3) known geotechnical/geological condition on the installed instrument sites; and (4) a database of actual recorded events acquired over time. The quality of these relationships are fundamental in obtaining hazard maps that reflect the seismic activity level and resulting hazard of the actual seismogenic zones modeled. In particular, if these relationships are biased towards a magnitude range or a distance-to-hypocenter range, outside of those ranges the predicted accelerations can be very inaccurate. A detailed discussion is presented elsewhere [6].

Large interplate earthquakes are the most important contributors to seismic hazard almost everywhere in Chile. Predicted spectral acceleration from these earthquakes is based on empirical published GMMs. Three GMMs with large ($M \geq 7.8$) subduction sources [43-45] are epistemically used in this project with different weights. The most recent of these models [45], uses data from the M=8.8 Maule source of 27 February 2010, and the M=9.0 Tohoku-Oki source of 11 March 2011, among many others. Some of the world's largest historical earthquakes, the M=9.5 Valdivia earthquake of 22 May 1960, the M=9.2 Alaska earthquake of 27 March 1964, and the M=9.2 Sumatra-Andaman Island earthquake of 26 December 2004 have few or no near-source strong-motion records. Thus, none of the GMMs are constrained by data associated with M>9.0 earthquakes. Fig. 8a-c shows source spectra for the three GMMs used in this project for rock site conditions, as defined by NCh433 (VS30=900 m/s). The top two red dashed curves correspond to magnitude 9.3 and 9.8, the latter being the maximum magnitude considered in this project. These curves represent extrapolations of empirical models where data are simply not available to constrain the model behavior (the dashed red lines emphasize this fact).

Three GMMs for intermediate-depth intraplate sources [43, 45-46] are epistemically used in this project with different weights. The earliest of these GMMs [46] has been corrected [47-48] and extrapolated from the published 3 s spectral period to 5 s (Fig. 8d-f).

Five GMMs for shallow crustal sources, including smaller (M<7.8) interface-zone earthquakes [49-53] are epistemically used in this project with equal weights. These models are the 2013 update of the Next Generation of Attenuation Models, a multi-year, five-team, multi-institution project led by the University of California's Pacific Earthquake Engineering Research Center in partnership with the USGS [54].

5. Results

5.1 Hazard from seismogenic zones

There are two interplate zones in the model, representing uncertainty in the location of the southern edge. There is no partition within these large zones. In each of these zones, the probabilistic ground motion tends to increase towards the center because the source scenarios exhibit more overlap towards the center. The modeled sources do not continue northwest of the northern edge, nor do they continue south of the southern edge. Fig. 9a shows the probabilistic PGA due to large interplate sources for events at 2% PE in 50 years (2%/50-yr). This figure shows the two models considered: one where the southeastern edge of the Nazca plate is the southern limit of rupture scenarios, and one where ruptures can occur beyond 45° S down to 52.5° S, where the southern edge of rupture scenarios continue well into the Antarctic plate. South-east of the southern end, most of the plate motion is taken up on the Magallanes-Lago Fagnano fault [19], not exhibited by these maps.

Fig. 9b shows the probabilistic PGA from South-zone sources at 2%/50-yr. This figure also shows the probabilistic PGA associated with Quaternary faults in Chile and neighboring areas in Argentina, Bolivia, and Peru. Some Quaternary faults that are in the model do not exhibit visible hazard at the 2,475-year return time used to obtain the map shown. Some examples of *invisible* sources are the San Ramón fault in central Chile and the Liquiñe-Ofqui fault system in the south part of Chile. A prominent visible fault system is the Lago Fagnano transform fault south of Punta Arenas. Low average slip rates on some of these faults result in mean recurrence intervals of major shocks much greater than the 2,475-year return time considered in the figure.

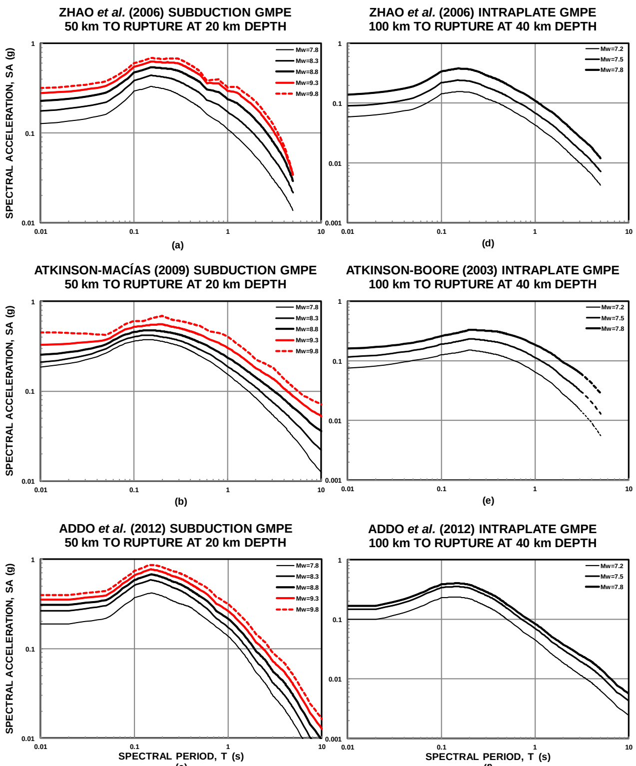

Figure 8 – Median 5% damped acceleration response spectra on rock from large-magnitude interplate and intraplate sources according to the GMMs developed by: (a) and (d) Zhao and others [43]; (b) Atkinson and Macías [44]; (c) and (f) Addo and others [45]; and (e) Atkinson and Boore [46-47]. Note: (b) and (d) include recommended corrections [48].

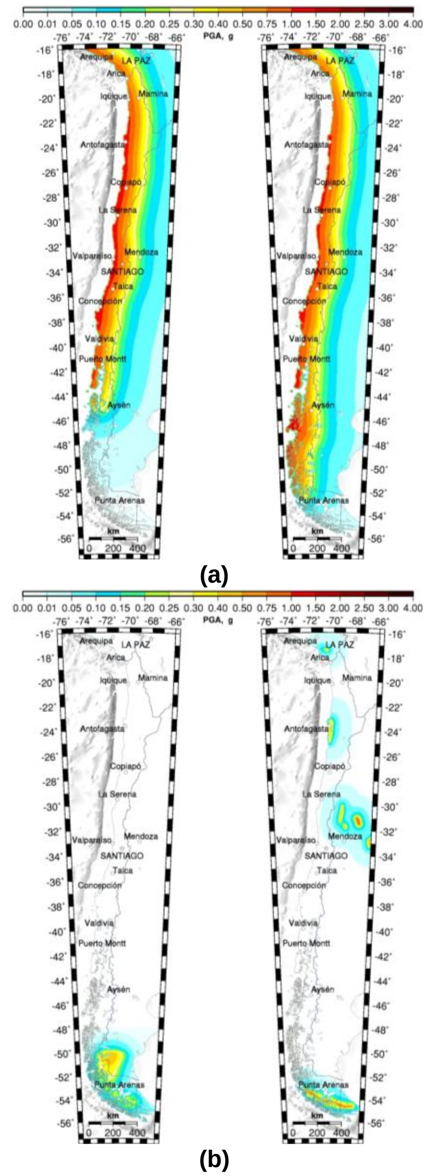

Figure 9 – Probabilistic PGA maps for Continental Chile at 2%/50-yr on rock. (a) PGA from subduction interplate sources with M=7.8-9.8. The left panel shows the map corresponding to the preferred logic-tree branch, whereas the right panel shows the map corresponding to the alternate logic-tree branch. (b) PGA from Southern Chile and Quaternary fault sources. The left panel corresponds to Southern Chile sources with M=5.0-8.0; there are also Quaternary faults in the south zone, but hazard from those sources is omitted on this map. The right panel corresponds to Quaternary fault sources.

Similarly, hazard maps for PGA and pSA, at different spectral periods, are obtained for the other considered seismogenic sources [6]: (a) shallow interplate, magnitudes 5.0 to 7.8; (b) shallow intraplate; (c) intermediate-depth and deep intraplate; and (d) outer-rise, affecting Insular Chile.

5.2 Total hazard in Continental Chile

Contributions from the various zones described above are combined by appropriately adding epistemic weighted hazard maps for different approximations which span the uncertainty in different features of the model [6].

Fig. 10 shows the onshore probabilistic motion associated with PGA and a number of pSA, for two levels of exceedance, 10% and 2% in 50-yr. Although not shown on the figures, hazard maps were also prepared for sites in Continental and Insular Chile, for the following spectral periods: 0.10 s (10 Hz), 0.15 s (6.66 Hz), 0.30 s (3.33 Hz), 0.40 s (2.5 Hz), 0.50 s (2 Hz), 0.75 s, 1.50 s, 2.00 s, 4.00 s, and 5.00 s. In total, thirteen hazard maps are available. Fig. 10 gives a sense of how the probabilistic motion varies with spectral period. The maps shown are for Chile and parts of neighboring countries. In particular, east of Copiapó from the north to Santiago on the south, the provinces of Mendoza and San Juan, located in Argentina, are the areas exhibiting Argentina's highest seismicity rates [55], where the slab does not subduct as steeply as in other areas (Fig. 2a), and where the probabilities of intermediate-depth seismic event occurrence are higher (Fig. 1).

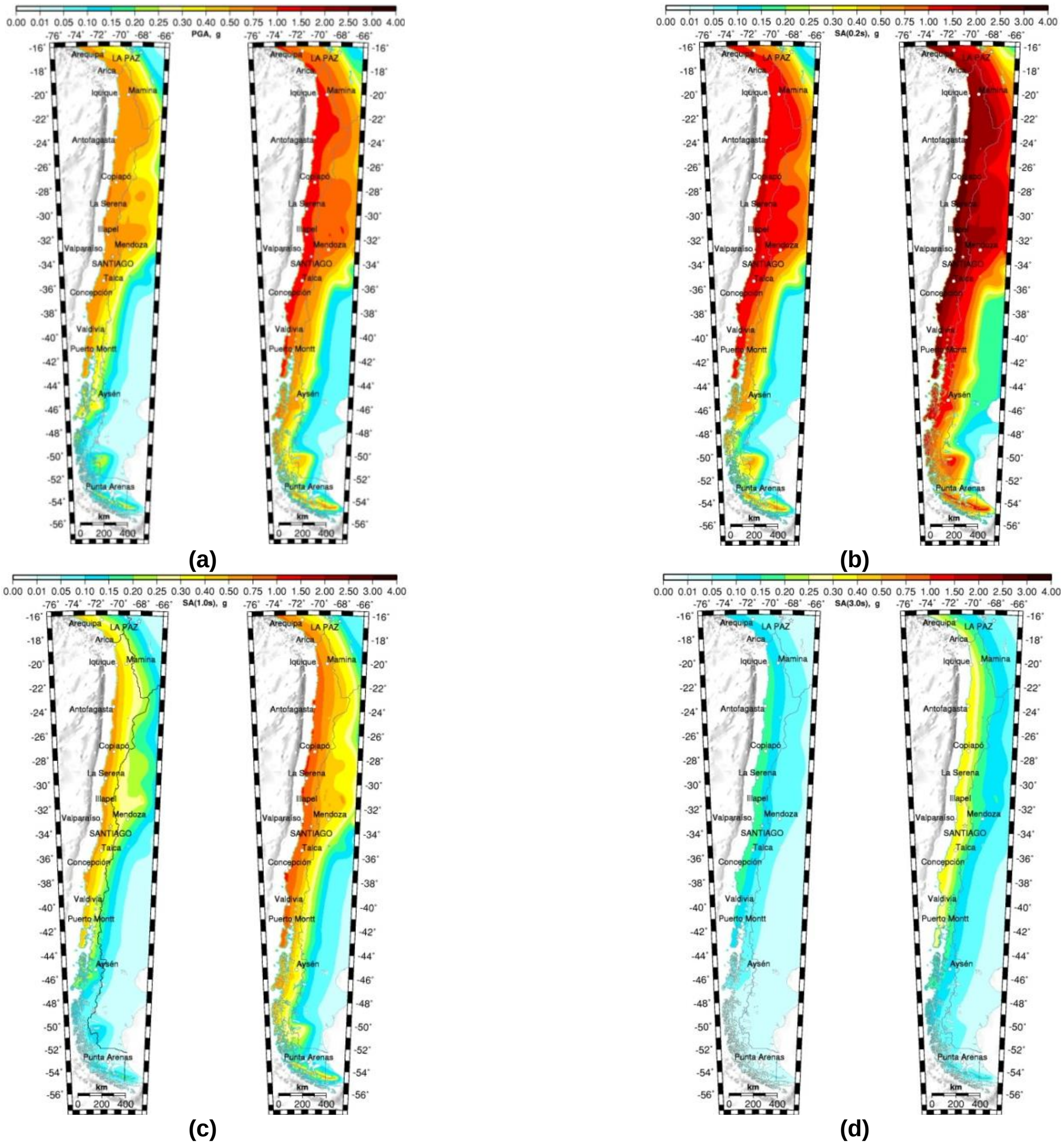

Figure 10 – Probabilistic ground motion maps for Continental Chile from all sources at 10% (left panels) and 2% (right panels) PE in 50 years on rock. (a) PGA. (b-d) pSA (5% critical damping) at 0.2, 1.0, and 3.0 s.

5.3 Total hazard in Insular Chile

Fig. 11a shows the probabilistic PGA in the vicinity of Easter and Salas y Gómez Islands, representing the total hazard from local sources. Other known sources are too distant to affect ground motion significantly on the islands. Fig. 11b shows the probabilistic PGA in the vicinity of the Juan Fernández Archipelago. Short-period hazard, such as PGA, is controlled by local seismicity south of these islands. For long-period hazard, large subduction events on the interface between the Nazca and South American plates, east of the archipelago, contribute significantly to seismic hazard. There is no cataloged seismicity for San Félix and San Ambrosio Islands (Desventuradas Archipelago). Hazard results from distant interface earthquakes with magnitudes greater than 7.8. PGA at 2%/50-yr on rock are 0.033g and 0.036g, respectively.

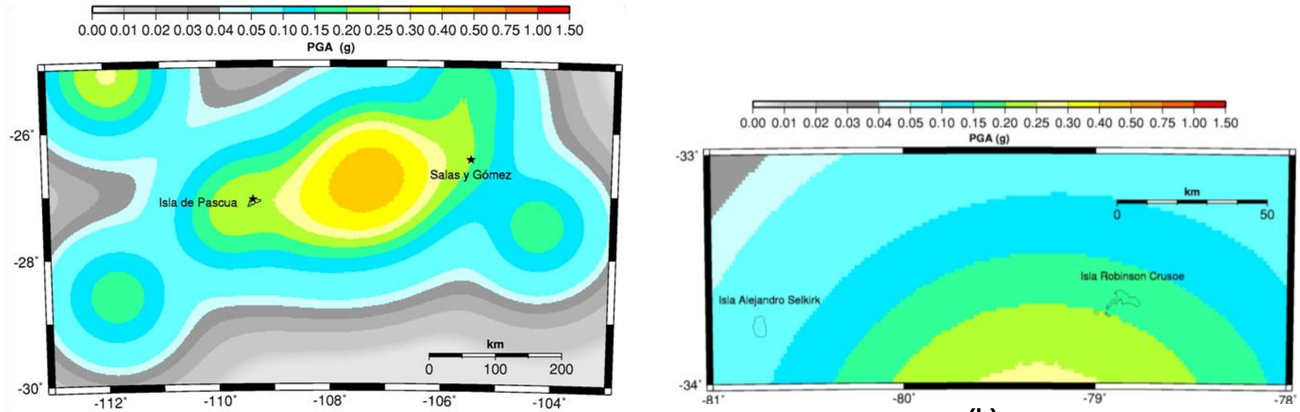

(a) (b)

Figure 11 – Probabilistic PGA map from all sources with M≥4 at 2%/50-yr on rock. (a) Easter and Salas y Gómez Islands, and vicinity. (b) Juan Fernández Archipelago and vicinity.

5.4 Applications

The hazard maps developed can be applied to: build a country seismic zonation to develop seismic design code criteria, improve seismic risk mitigation efforts, evaluate the risk of insured portfolios distributed over the national territory, and help authorities make public policy decisions, among other uses.

5.4.1 Hazard disaggregation in Iquique for the 01 April 2014 earthquake. Details on the seismic hazard at a site can be obtained using source disaggregations, displaying the relative contributions of various hazardous sources [56]. A common way is to show relative contributions (to ground motion exceedances) as a function of magnitude, distance, and ground-motion uncertainty, ε_0 [57-58]. Fig. 12 shows the PGA disaggregation of the 100-year return period at Iquique Regional Hospital. An earthquake M=8.2 struck on 01 April 2014. The maximum PGA recorded by an accelerometer installed at the site (IQUI) was 0.32g [59]. The 100-year PGA is 0.353 according to the PSHA model, or 10.3% greater than the recorded PGA. Nazca plate subduction sources with a range of magnitudes correspond to the most likely sources to produce exceedances of this ground acceleration (the tallest columns on Fig. 12).

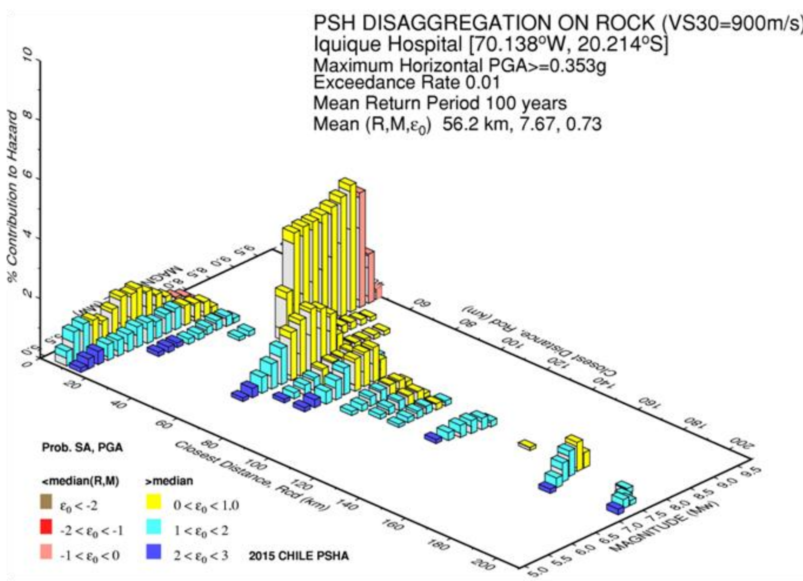

Figure 12 – Disaggregation of a 100-year PGA at Iquique Regional Hospital.

5.4.2 Probabilistic spectra for Arica, Santiago, Concepción, and Valdivia. Fig. 13a shows the probabilistic spectra at rock sites in Arica, Santiago, Concepción, and Valdivia, all associated with the 10%/50-yr, or 475-year mean return period. The figure also shows the corresponding Chilean seismic code design spectra on rock in zone 3 for buildings [1, 5], industrial installations [2], and transportation infrastructure [3]. It may be observed that the 10%/50-yr spectra match well the building code spectra shape, but at higher values, and the maxima occur at a shorter period, but close. This is expected. In effect, the spectra calculated by the methods presented on this report are derived from the geometric average of the two horizontal peak ground spectral accelerations which is higher than the maximum effective ground acceleration coefficient, A_0, given by the code. Effective maximum acceleration can be as much as $\sqrt{2}$ times higher than the maximum amplitude of a seismic wave. Once this factor is accounted for (Fig. 13b), with the exception of Concepción, the other cities' spectra values are lower than the building code spectrum for short periods (T<0.5 s), and higher for longer periods. The Concepción spectrum is higher than the building code spectrum throughout the period range sampled. It must be noted that for longer periods the spectral values are larger, much markedly for Concepción, showing the contributions to higher spectral periods of the long duration earthquakes occurring in Chile. The "real" spectrum lays between the spectra shown on Fig. 14a and 14b, closer to the latter.

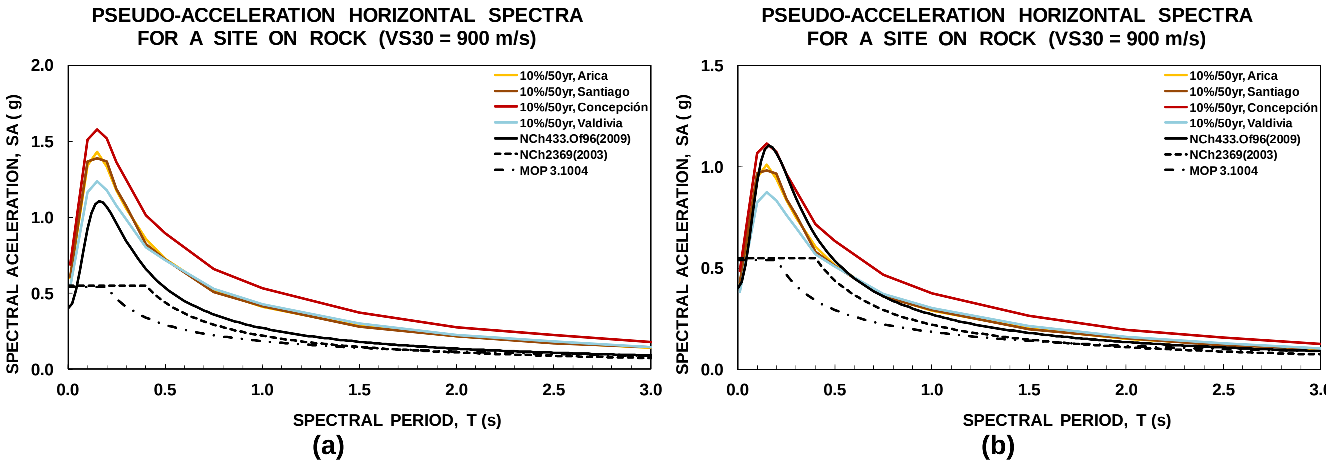

Figure 14 – Probabilistic site spectra for 5% damped spectral response acceleration with 10%/50-yr on rock, using the M_{max}=9.8 model, in Arica [18.50° S, 70.30° W], Santiago [33.40° S, 70.60° W], Concepción [36.80° S, 73.00° W], and Valdivia [39.80° S, 73.20° W]. (a) Spectra from hazard model calculations. (b) Spectra corrected by a √2 factor.

6. Conclusions

Seismic hazard maps were obtained for Continental and Insular Chile using the latest scientific and seismology knowledge and state-of-the-art methodologies, widely accepted by both seismologists and engineers. These procedures have closely followed the methodology used by the USGS to develop and update USA's National Seismic Hazard Mapping Project. These maps can provide the basis for many public and private policies regarding earthquakes, including seismic-design regulations for buildings, bridges, highways, railroads, and other public and private infrastructure. These maps could be incorporated into building codes to allow for proper design of new infrastructure, and adequate seismic rehabilitation of old infrastructure designed with outdated codes; hence, allowing for prudent allocation of resources by reducing conservative designs in areas deemed of unrealistic high seismic demand by old codes.

These hazard maps are the first complete set of such maps developed for Chile using modern seismology-based hazard analysis and methods. The current hazard maps, shown in the seismic codes, do not provide a good basis for comparison. However, the seismic acceleration design spectra defined by these codes can be compared with the maps developed for a 10%/50-yr. The comparison made for a few sites show different seismic demand for each site, and slightly above the acceleration design spectra prescribed by the codes, particularly at longer periods, accounting for the long duration of mega-thrust events affecting Chile. On the other hand, observations of actual data provided after the 2005 Tarapacá, 2010 Maule, and 2014 Iquique earthquakes show good correlation with the results obtained using the model for similar earthquake scenarios.

7. Acknowledgements

The sponsorship of the Association of Chilean Insurers (*Asociación de Aseguradores de Chile*) is gratefully acknowledged. Dr. Charles S. Mueller from the USGS provided valuable comments. This project has benefitted immensely from the work developed by the USGS's NSHMP, using theory, methodologies, and software developed over the years by AD Frankel, SC Harmsen, CS Mueller, MD Petersen, RL Wesson, and others. Dr. Mark D. Petersen, the current NSHMP Project Chief, provided continuous encouragement. The help provided by

Mr. Héctor Massone from the National Seismological Center of the University of Chile in compiling the seismological data is acknowledged.

8. References

[1] INN (2009): *Diseño Sísmico de Edificios*, Norma Chilena Oficial NCh 433.Of1996 (Modificada en 2009), Instituto Nacional de Normalización, Santiago, Chile (2ª edición).

[2] INN (2003): *Diseño Sísmico de Estructuras e Instalaciones Industriales*, Norma Chilena Oficial NCh 2369.Of2003, Instituto Nacional de Normalización, Santiago, Chile.

[3] Dirección de Vialidad (2013): 'Instrucciones y criterios de diseño,' **3**, *Manual de Carreteras*, Ministerio de Obras Públicas, Santiago, Chile (Junio 2002, edición 2013).

[4] República de Chile (2011): 'Aprueba reglamento que fija el diseño sísmico de edificios,' *Diario Oficial de la República de Chile*, Cuerpo **I**, 8-12 (25 February).

[5] República de Chile (2011): 'Aprueba reglamento que fija el diseño sísmico de edificios y deroga Decreto Nº 117, de 2010,' *Diario Oficial de la República de Chile*, Cuerpo **I**, 5-7 (13 December).

[6] Medina F, Harmsen SC, Barrientos SE (2015): *Proyecto Mapa de Riesgo Sísmico de Chile. Módulo 2A: Amenaza Sísmica*, informe para Asociación de Aseguradores de Chile, FME Engineering, San Francisco, California, USA.

[7] Silgado E (1985): 'Terremotos destructivos en América del Sur 1530-1894,' *Programa para la Mitigación de los Efectos de los Terremotos en la Región Andina (Proyecto SISRA)*, **10**, Centro Regional de Sismología para América del Sur (CERESIS), Lima, Perú.

[8] ICC (2012): *International Building Code*, International Code Council, Inc., Washington, DC, USA.

[9] Structural Engineering Institute (2013): *ASCE/SEI 7 Minimum Design Loads For Building and Other Structures – 2016 Development Cycle*, American Society of Civil Engineers, Reston, Virginia, USA. {http://www.asce.org/sei/Content.aspx?id=23622324319} [24 August 2013]

[10] Cornell CA (1968): 'Engineering seismic risk analysis,' *Bulletin of the Seismological Society of America*, **58**, 1583-1606.

[11] Frankel A (1995): 'Mapping seismic hazard in the Central and Eastern United States,' *Seismological Research Letters*, **66**(4), 8-21.

[12] Petersen MD, Moschetti MP, Powers PM, Mueller CS, Haller KM, Frankel AD, Zeng Y, Rezaeian S, Harmsen SC, Boyd OS, Field N, Chen R, Rukstales KS, Luco N, Wheeler RL, Williams RA, Olsen AH (2014): 'Documentation for the 2014 update of the United States national seismic hazard maps,' *Open-File Report 2014-1091*, US Geological Survey, Department of the Interior, Reston, Virginia, USA.

[13] Petersen M, Harmsen S, Haller K, Mueller C, Luco N, Hayes G, Dewey J, Rukstales K (2011): 'Preliminary seismic hazard model for South America,' in *La Sismología en Sudamérica y los Mecanismos de Prevención y Mitigación del Peligro y Riesgo Sísmico. Homenaje a Alberto Giesecke* (D Huaco, editor), 227-231, Asociación Andrés del Castillo y Centro Regional de Sismología para América del Sur (CERESIS), Lima, Perú. {http://earthquake.usgs.gov/hazards/products/foreign/SAmer-Proceedings2010.pdf} [18 September 2015]

[14] Leyton F, Ruiz S, Sepúlveda SA (2009): 'Preliminary re-evaluation of probabilistic seismic hazard assessment in Chile: from Arica to Taitao Peninsula,' *Advances in Geosciences*, **22**, 147-153.

[15] Núñez I, Boroschek R, Comte D, Contreras V (2015): 'Nuevo peligro sísmico para Chile,' paper 189, *XI Congreso Chileno de Sismología e Ingeniería Sísmica ACHISINA 2015*, Santiago, Chile (18-20 March).

[16] Bommer JJ, Abrahamson NA, Strasser FO, Pecker A, Bard P-Y, Bungum H, Cotton F, Fäh D, Sabetta F, Scherbaum F, Studer J (2004): 'The challenge of defining upper bounds on earthquake ground motions,' *Seismological Research Letters*, **75**, 82-95.

[17] Barrientos SE (2007): 'Earthquakes in Chile,' in *The Geology of Chile* (T Moreno, W Gibbons, editors), 263-287, Geological Society of London, London, United Kingdom.

[18] Hayes GP, Wald DJ, Johnson RL (2012): 'Slab1.0: A three-dimensional model of global subduction zone geometries,' *Journal of Geophysical Research: Solid Earth*, **117**, B01302.

[19] Costa CH, Smalley, Jr., C, Schwartz DP, Stenner HD, Ellis M, Ahumada EA, Velasco MS (2006): 'Paleoseismic observations of an onshore transform boundary: The Magallanes-Fagnano Fault, Tierra del Fuego, Argentina,' *Revista de la Asociación Geológica Argentina*, **61**, 647-657.

[20] Lavenu A, Thiele R, Machette MN, Dart RL, Bradley L-A, Haller KM (2000): 'Maps and database of Quaternary

faults in Bolivia and Chile,' *Open-File Report 00-283*, US Geological Survey, Golden, Colorado, USA.

[21] Costa CH, Audemard FA, Bezerra FHR, Lavenu A, Machette MN, París G (2006): 'An overview of the main Quaternary deformation of South America,' *Revista de la Asociación Geológica Argentina*, **61**, 461-479.

[22] Rauld RA (2011): 'Deformación cortical y peligro sísmico asociado a la falla San Ramón en el frente cordillerano de Santiago, Chile Central (33° S),' *tesis de Doctor en Ciencias*, Facultad de Ciencias Físicas y Matemáticas, Universidad de Chile, Santiago, Chile.

[23] Costa CH, Machette MN, Dart RL, Bastias HE, Paredes JD, Perucca LP, Tello JE, Haller KM (2000): 'Map and database of Quaternary faults and folds in Argentina,' *Open-File Report 00-0108*, US Geological Survey, Golden, Colorado, USA.

[24] Macharé J, Fenton CH, Machette MN, Lavenu A, Costa C, Dart RL (2000): 'Database and map of Quaternary faults and folds in Perú and its offshore region,' *Open-File Report 03-451*, US Geological Survey, Golden, Colorado, USA.

[25] Gutenberg B, Richter CF (1944): 'Frequency of earthquakes in California,' *Bulletin of the Seismological Society of America*, **34**, 185-188.

[26] Gardner JK, Knopoff L (1974): 'Is the sequence of earthquakes in Southern California, with aftershocks removed, Poissonian?,' *Bulletin of the Seismological Society of America*, **64**, 1363-1367.

[27] Wesson RL, Boyd OS, Mueller CS, Bufe CG, Frankel AD, Petersen MD (2007): 'Revision of time-independent probabilistic seismic hazard maps for Alaska,' *Open-File Report 2007-1043*, US Geological Survey, Reston, Virginia, USA.

[28] Farías M, Comte D, Roecker S, Carrizo D, Pardo M (2011): 'Crustal extensional faulting triggered by the 2010 Chilean earthquake: The Pichilemu Seismic Sequence,' Tectonics, **30**(6), TC6010.

[29] Ryder I, Rietbrock A, Kelson K, Bürgmann R, Floyd M, Socquet A, Vigny C, Carrizo D (2012): 'Large extensional aftershocks in the continental forearc triggered by the 2010 Maule earthquake, Chile,' *Geophysical Journal International*, **188**, 879-890.

[30] Stepp JC (1972): 'Analysis of Completeness of the Earthquake Sample in the Puget Sound Area and its effect on statistical estimates of earthquake Hazard,' *International Conference on Microzonation for Safer Construction Research and Application*, 897-909, Seattle, Washington, USA (30 October - 03 November).

[31] Lomnitz C (2004): 'Major earthquakes of Chile: A historical survey, 1535-1960,' *Seismological Research Letters*, **75**, 368-378.

[32] Barrientos SE, Ward SN (1990): 'The 1960 Chile earthquake: Inversion from slip distribution from surface deformation,' *Geophysical Journal International*, **103**, 589-598.

[33] Russo RM, VanDecar JC, Comte D, Mocanu VI, Gallego A, Murdie RE (2010): 'Subduction of the Chile Ridge: Upper mantle structure and flow,' *GSA Today*, **20**(9), 4-10.

[34] Coppersmith K, DiSilvestro L, Hansen K, Wells D, Youngs RR (1995): *Seismic Design Mapping, State of Oregon*, Final Report, project 2442, Geomatrix Corporation, prepared for Oregon Department of Transportation, Salem, Oregon, USA.

[35] Strasser FO, Arango MC, Bommer JJ (2010): 'Scaling of the source dimensions of interface and intraslab subduction-zone earthquakes with moment magnitude,' *Seismological Research Letters*, **81**, 941-950.

[36] Papazachos BC, Scordilis EM, Panagiotopoulos DG, Papazachos CB, Karakaisis GF (2004): 'Global relations between seismic fault parameters and moment magnitude of earthquakes,' *Bulletin of the Geological Society of Greece*, **VI**, 1482-1489.

[37] Melnick D, Bookhagen B, Strecker MR, Echtler HP (2009): 'Segmentation of mega-thrust rupture zones from fore-arc deformation patterns over hundreds to millions of years, Arauco peninsula, Chile,' *Journal of Geophysical Research: Solid Earth*, **114**(B1), B01407.

[38] Christensen DH, Beck SL (1994): 'The rupture process and tectonic implications of the Great 1964 Prince William Sound Earthquake, *Pure and Applied Geophysics*, **142**, 29-53.

[39] Ruegg JC, Campos J, Armijo R, Barrientos S, Briole P, Thiele R, Arancibia M, Cañuta J, Duquesnoy T, Chang M, Lazo D, Lyon-Caen H, Ortlieb L, Rossignol JC, Serrurier L (1996): 'The M_w=8.1 Antofagasta (North Chile) Earthquake of July 30, 1995: First results from teleseismic and geodetic data,' *Geophysical Research Letters*, **23**, 917-920.

[40] Vigny C, Socquet A, Peyrat S, Ruegg J-C, Métois M, Madariaga R, Morvan S, Lancieri M, Lacassin R, Campos J, Carrizo D, Bejar-Pizarro M, Barrientos S, Armijo R, Aranda C, Valderas-Bermejo M-C, Ortega I, Bondoux F,

Baize S, Lyon-Caen H, Pavez A, Vilotte JP, Bevis M, Brooks B, Smalley R, Parra H, Baez J-C, Blanco M, Cimbaro S, Kendrick E (2011): 'The 2010 M_w 8.8 Maule Megathrust Earthquake of Central Chile, monitored by GPS,' *Science*, **332**, 1417-1421.

[41] Bilek SL, Lay T (2000): 'Depth dependent rupture properties in circum-Pacific subduction zones,' in *GeoComplexity and the Physics of Earthquakes, Geophysical Monograph 120* (JB Rundle, DL Turcotte, W Klein, editors), 165-186, American Geophysical Union, Washington, DC, USA.

[42] Douglas J (2011): 'Ground-motion prediction equations 1964–2010,' *PEER 2011/102, Pacific Earthquake Engineering Research Center*, University of California, Berkeley, USA.

[43] Zhao JX, Zhang J, Asano A, Ohno Y, Oouchi T, Takahashi T, Ogawa H, Irikura K, Thio HK, Somerville PG, Fukushima Y, Fukushima Y (2006): 'Attenuation relations of strong ground motion in Japan using site classification based on predominant period,' *Bulletin of the Seismological Society of America*, **96**, 898-913.

[44] Atkinson GM, Macias M (2009): 'Predicted ground motions for great interface earthquakes in the Cascadia subduction zone,' *Bulletin of the Seismological Society of America*, **99**, 1552-1578.

[45] Addo KO, Abrahamson NA, Youngs RR (2012): 'Probabilistic seismic hazard analysis (PSHA) model Volume 3: Ground motion characterization (GMC) model,' *report E658, BC Hydro*, Vancouver, British Columbia, Canada.

[46] Atkinson GM, Boore DM (2003): 'Empirical ground-motion relations for subduction-zone earthquakes and their application to Cascadia and other regions,' *Bulletin of the Seismological Society of America*, **93**, 1703-1729.

[47] Atkinson GM, Boore DM (2008): Erratum to 'Empirical ground-motion relations for subduction-zone earthquakes and their application to Cascadia and other regions,' *Bulletin of the Seismological Society of America*, **98**, 2567-2569.

[48] Boore DM, Atkinson GM (2008): 'Ground-motion prediction equations for the average horizontal component of PGA, PGV, and 5%-damped PSA at spectral periods between 0.01 s and 10.0 s,' *Earthquake Spectra*, **24**, 99-138.

[49] Abrahamson NA, Silva WJ, Kamai R (2013): 'Update of the AS08 ground-motion prediction equations based on the NGA-West2 data set,' *PEER 2013/04, Pacific Earthquake Engineering Research Center*, University of California, Berkeley, USA.

[50] Boore DM, Stewart JP, Seyhan E, Atkinson GA (2013): 'NGA-West2 equations for predicting response spectral accelerations for shallow crustal earthquakes,' *PEER 2013/05, Pacific Earthquake Engineering Research Center*, University of California, Berkeley, USA.

[51] Campbell KW, Bozorgnia Y (2013): 'NGA-West2 Campbell-Bozorgnia ground motion model for the horizontal components of PGA, PGV, and 5%-damped elastic pseudo-acceleration response spectra for periods ranging from 0.01 to 10 sec,' *PEER 2013/06, Pacific Earthquake Engineering Research Center*, University of California, Berkeley, USA.

[52] Chiou BSJ, Youngs RR (2013): 'Update of the Chiou and Youngs NGA ground motion model for average horizontal component of peak ground motion and response spectra,' *PEER 2013/07, Pacific Earthquake Engineering Research Center*, University of California, Berkeley, USA.

[53] Idriss IM (2013): 'NGA-West2 model for estimating average horizontal values of pseudo-absolute spectral accelerations generated by crustal earthquakes,' *PEER 2013/08, Pacific Earthquake Engineering Research Center*, University of California, Berkeley, USA.

[54] Stewart JP, Archuleta RJ, Power MS, editors (2008): 'Special issue on the Next Generation Attenuation Project,' *Earthquake Spectra*, **24**, 1-341.

[55] Perucca LP, Moreiras SM (2006): 'Liquefaction phenomena associated with historical earthquakes in San Juan and Mendoza Provinces, Argentina,' *Quaternary International*, **158**, 96-109.

[56] Harmsen S, Frankel A (2001): 'Geographic deaggregation of seismic hazard in the United States,' *Bulletin of the Seismological Society of America*, **91**, 13-26.

[57] McGuire RK (1995): 'Probabilistic seismic hazard analysis and design earthquakes: Closing the loop,' *Bulletin of the Seismological Society of America*, **85**, 1275-1284.

[58] Harmsen SC (2001): 'Mean and modal ε in the deaggregation of probabilistic ground motion,' *Bulletin of the Seismological Society of America*, **91**, 1537-1552.

[59] Boroschek R, Soto P (2014): 'Terremoto Norte Chile – 1 de Abril de 2014 Mw=8.2,' *Informe Preliminar N°1, Departamento de Ingeniería Civil*, Universidad de Chile, Santiago, Chile.